

Article

# Cavitation Erosion Resistance and Wear Mechanism Model of Flame-Sprayed $\text{Al}_2\text{O}_3$ -40% $\text{TiO}_2$ /NiMoAl Cermet Coatings

Mirośław Szala \*  and Tadeusz Hejwowski

Department of Materials Engineering, Faculty of Mechanical Engineering, Lublin University of Technology, Nadbystrzycka 36D, 20-618 Lublin, Poland; t.hejwowski@pollub.pl

\* Correspondence: m.szala@pollub.pl; Tel.: +48-815-384-209

Received: 5 June 2018; Accepted: 19 July 2018; Published: 21 July 2018



**Abstract:** This manuscript deals with the cavitation erosion resistance of flame-sprayed  $\text{Al}_2\text{O}_3$ -40% $\text{TiO}_2$ /NiMoAl cermet coatings (low-velocity oxy-fuel (LVOF)), a new functional application of cermet coatings. The aim of the study was to investigate the cavitation erosion mechanism and determine the effect of feedstock powder ratio ( $\text{Al}_2\text{O}_3$ - $\text{TiO}_2$ /NiMoAl) of LVOF-sprayed cermet coatings on their cavitation erosion resistance. As-sprayed coatings were investigated for roughness, porosity, hardness, and Young's modulus. Microstructural characteristics of the cross section and the surface of as-sprayed coatings were examined by light optical microscopy (LOM), scanning electron microscopy (SEM) with energy-dispersive X-ray spectroscopy (EDS) and X-ray diffraction (XRD) methods. Coating cavitation tests were conducted in accordance with the ASTM G32 standard using an alternative stationary specimen testing method with usage of reference samples made from steel, copper, and aluminum alloys. Cavitation erosion resistance was measured by weight and volume loss, and normalised cavitation erosion resistance was calculated. Surface eroded due to cavitation was examined in successive time intervals by LOM and SEM-EDS. On the basis of coating properties and cavitation investigations, a phenomenological model of the cavitation erosion of  $\text{Al}_2\text{O}_3$ -40% $\text{TiO}_2$ /NiMoAl cermet coatings was elaborated. General relationships between their properties, microstructure, and cavitation wear resistance were established. The  $\text{Al}_2\text{O}_3$ -40% $\text{TiO}_2$ /NiMoAl composite coating containing 80% ceramic powder has a higher cavitation erosion resistance than the reference aluminium alloy.

**Keywords:** cermet coating; alumina–titania; thermal spraying; flame spraying; cavitation erosion; microstructure; wear model

## 1. Introduction

Alumina–titania sprayed coatings,  $\text{Al}_2\text{O}_3$ - $\text{TiO}_2$ , are used in the chemical engineering, metal, and paper industries to improve resistance to wear, corrosion, and high-temperature oxidation [1–6]. The protective  $\text{Al}_2\text{O}_3$ - $\text{TiO}_2$  ceramic coatings are typically deposited with 3% [5,7,8], 13% [1,3,8–10], 20% [3], 40% [2,3], or 50% [11] addition of  $\text{TiO}_2$ . Apart from the fact that plasma spraying (PS) is the most widely used technique of  $\text{Al}_2\text{O}_3$ - $\text{TiO}_2$  ceramic deposition [3,7,8,11,12], processes like flame spraying (low-velocity oxy-fuel LVOF) [2,5,6], high-velocity oxy-fuel (HVOF) [12], or even laser cladding [1] are also employed. Among the above processes, LVOF is a low-power-consuming and, thus, cost-effective method, as compared with other thermal spraying techniques [2,9]. In addition, the  $\text{Al}_2\text{O}_3$ - $\text{TiO}_2$  sprayed coating structure produced by PS or HVOF [13,14] is well described in the literature. However, data about the microstructure and properties of alumina–titania coatings deposited by LVOF spray processes are rarely reported [15].

In industrial applications, different metallic bond coats such as NiAl, NiCr, NiCrAl, NiMoAl, or NiCrMo are employed to increase ceramic coating adhesion to the substrate [4,8,14,16]. Coatings deposited with NiMoAl feedstock powders are described in the literature as promoting high bonding strength, good antioxidation ability, and excellent corrosion and wear resistance, and are widely used as a protective coating for many industrial components under high-temperature conditions [17]. On the whole, functional properties of both ceramic  $\text{Al}_2\text{O}_3\text{-TiO}_2$  and metallic NiMoAl coatings are complementary, and it seems justified to manufacture composite coatings deposited by LVOF spraying that combine the beneficial properties of  $\text{Al}_2\text{O}_3\text{-TiO}_2$  and NiMoAl coatings. Nevertheless, the influence of the microstructure of LVOF-sprayed cermet coatings with a blend of  $\text{Al}_2\text{O}_3\text{-TiO}_2$  and NiMoAl feedstock powders on their cavitation erosion resistance has not been reported.

The results of the cavitation erosion of various sprayed coatings (WC-Co, CrC, or NiAl coatings) are usually reported in reference to bulk metal alloys [18,19]; a survey of the literature of the subject indicates that the cavitation erosion resistance (CER) of alumina–titania ceramics manufactured by LVOF spraying has been inadequately examined. The literature offers the studies of coatings with 13%  $\text{TiO}_2$  addition fabricated only by PS or HVOF [10,12], and the results are usually presented without using any reference bulk metals. As a result, it is difficult to interpret the results and examine the applications of  $\text{Al}_2\text{O}_3\text{-TiO}_2$  coatings. Moreover, the literature survey reveals that only few studies focus on the microstructure and wear resistance properties of cermet coatings, e.g.,  $\text{Cr}_3\text{C}_2\text{-NiCr/Ni}$  [20], WC-Co/Cr-NiCrFeBSiC [21], and  $\text{Al}_2\text{O}_3\text{-TiO}_2\text{/NiMoAl}$  [15] cermet coatings. Nevertheless, the cavitation erosion resistance of LVOF-sprayed  $\text{Al}_2\text{O}_3\text{-TiO}_2\text{/NiMoAl}$  composite coatings have not been previously identified; hence, it seems worth investigating new functional applications of these coatings. Additionally, it seems justified determining the content ratio of metallic (NiMoAl) to ceramic feedstock powder ( $\text{Al}_2\text{O}_3\text{-40}\%\text{TiO}_2$ ) that will ensure the deposition of composite coating  $\text{Al}_2\text{O}_3\text{-40}\%\text{TiO}_2\text{/NiMoAl}$  with potentially beneficial CER properties.

This manuscript investigates the cavitation erosion resistance and properties of LVOF-sprayed  $\text{Al}_2\text{O}_3\text{-40}\%\text{TiO}_2\text{/NiMoAl}$  cermet coatings. Deposited coatings have never been examined in relation to their cavitation erosion resistance. The study verifies a new solution for cavitation wear prevention. The aim of the work is to assess the cavitation erosion resistance and wear mechanism of LVOF-sprayed  $\text{Al}_2\text{O}_3\text{-40}\%\text{TiO}_2\text{/NiMoAl}$  cermet coatings as well as to determine the effect of feedstock powder ratios ( $\text{Al}_2\text{O}_3\text{-TiO}_2\text{/NiMoAl}$ ) of LVOF-sprayed composite coatings on cavitation erosion resistance.

## 2. Material and Methods

### 2.1. Coating Manufacturing

The objects of our investigation were cermet coatings ( $\text{Al}_2\text{O}_3\text{-40}\%\text{TiO}_2\text{/NiMoAl}$ ) sprayed with the flame powder spray method (LVOF) with different weight fractions of ceramic powder (% cp) and metallic powder (% mp). Properties of the metallic powder (mp) and the ceramic powder (cp) are given in Table 1. According to manufacturer's data, the AMI 3452.6 (NiMoAl) powder is intended to be used as a bond coat, while the MX 6-3018 ( $\text{Al}_2\text{O}_3\text{-40}\%\text{TiO}_2$ ) powder is applicable for low-roughness and high-resistance-to-wear coatings used in the textile industry or for preventing the wear of pump seals. The powders vary in grain size and morphology, as described in Table 1 and Figure 1.

Table 1. Feedstock powder materials.

Type of Powder (Description)	Powder Grade	Nominal Chemical Composition (wt %)	Grain Size ( $\mu\text{m}$ )
Metallic powder (mp)	AMI 3452.6	Al = 5.2%; Mo = 4.9%; Fe = 0.8%; Si = 0.4%, Ni, bal.	−125 + 45
Ceramic powder (cp)	MX 6-3018.2	$\text{Al}_2\text{O}_3\text{-40}\%\text{TiO}_2$	−40 + 15

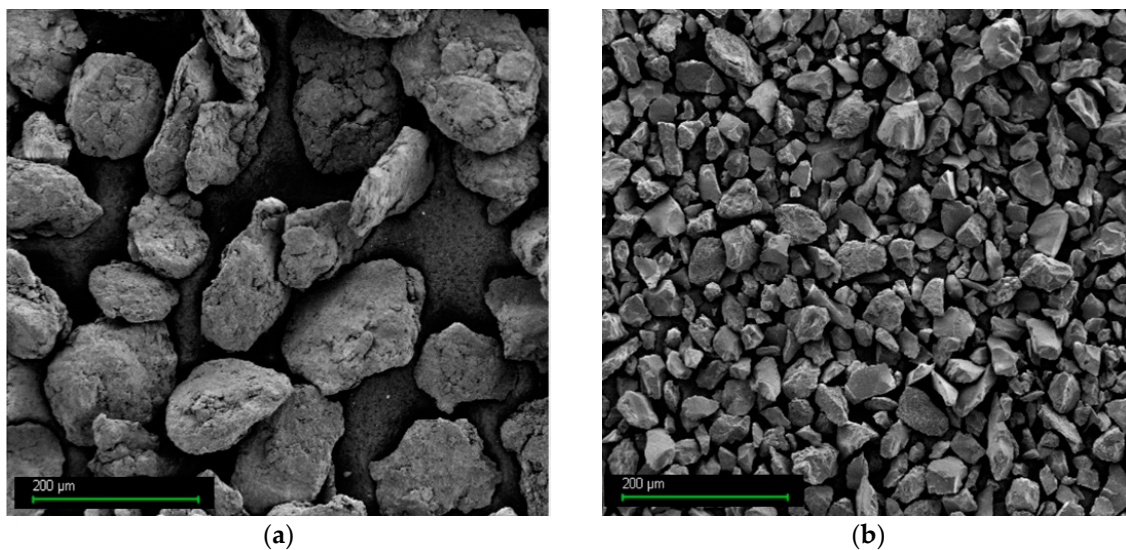


**Figure 1.** Feedstock powders, SEM: (a) NiMoAl metallic powder and (b) Al<sub>2</sub>O<sub>3</sub>-40%TiO<sub>2</sub> ceramic powder.

Coatings were LVOF sprayed by means of the UTP Uni-Spray-Jet torch (GTV Verschleiss-Schutz GmbH, Germany). Feedstock powders were delivered to the torch in the argon stream from the feeding station, in which the powder material was kept in fluidized condition [22]. Coatings were deposited on the face of  $\varnothing 25 \times 55$  mm cylinders made of mild steel grade S235JR ( $C = 0.23\%$ ). The deposition parameters of metallic bond coat were spraying nozzle, USJ-N; powder nozzle, N; oxygen pressure, 0.3 MPa; acetylene pressure, 0.07 MPa; and standoff distance, 200 mm. Meanwhile, parameters of ceramic-containing coats were spraying nozzle, USJ-HT; powder nozzle, S; oxygen pressure, 0.3 MPa; acetylene pressure, 0.07 MPa; and standoff distance, 180 mm. Prior to spraying, the steel substrate was sand blasted with 70 mesh corundum to  $Ra = 15.2 \mu\text{m}$ . Eleven steel coupons were deposited with different types of coating systems. The first coupon was sprayed only with NiMoAl metallic powder (mp) and to a coating thickness of about 250  $\mu\text{m}$ . Another ten substrates were sprayed with mp bond coats of approximately 100  $\mu\text{m}$  thickness and then sprayed with different cermet top layers. Nine top coats were deposited with the blends of cp and mp (Al<sub>2</sub>O<sub>3</sub>-40%TiO<sub>2</sub> and NiMoAl powders) sprayed with a gradual addition of 10% ceramic powder ranging from 10% to 90% of cp. Each subsequent cermet sample was produced with a 10% higher content of the ceramic powder than the previous. A 100% cp top layer was deposited onto the previously deposited bond coat. The thickness of the top coats was about 200  $\mu\text{m}$  (total coating thickness equals approximately 300  $\mu\text{m}$ ).

## 2.2. Characterization Techniques

As-sprayed coatings were examined for hardness, microstructure, and phase composition with light optical microscopy (LOM), scanning electron microscopy with energy-dispersive X-ray spectroscopy (SEM-EDS), and phase X-ray diffraction (XRD). The composite structure of Al<sub>2</sub>O<sub>3</sub>-TiO<sub>2</sub>/NiMoAl coatings was studied on the cross section by means of LOM (Nikon MA200, Nikon Corporation). The porosity of sprayed coatings was measured with the ImagePro computer image analysis software (Media Cybernetics, Inc., USA) and ten photos per sample were evaluated. Nanohardness measurements were conducted by means of a nanoindentation tester (CSM Instruments, USA) with a load of 150 mN and a dwelling time of 10 s. Elastic modulus calculations were based on a modified Oliver and Pharr approach with Poisson's ratio set equal to 0.3. The coatings were examined by the X-ray diffraction measurement method (XRD) using a Philips PW1850 diffractometer (PANalytical, Eindhoven, The Netherlands) with Cu K $\alpha$  radiation. As-sprayed coating surface morphology was investigated with both the SEM-EDS method using Phenom World Pro-X (15 kV, BSE detector, Phenom-World) and surface profilometer methods. The Surtronic tester profilometer (Taylor

Hobson, UK) was used to measure surface roughness of the samples. The coating average surface roughness parameter ( $R_a$ ) value was defined according to the ISO 4287:1997 standard [23].

### 2.3. Cavitation Erosion Testing

A set of as-sprayed  $\text{Al}_2\text{O}_3$ -40% $\text{TiO}_2$ /NiMoAl coating specimens with the dimensions of  $\varnothing 25 \times 5$  mm were machined from sprayed cylinders and then subjected to cavitation tests. According to data on cavitation erosion in the cited literature, steels, copper, and aluminium alloys are usually used as standard reference materials. Hence, in our experiment, the reference coupons were manufactured from these structural alloys, as presented in Table 2. This will facilitate a comparison of results obtained for the sprayed  $\text{Al}_2\text{O}_3$ -40% $\text{TiO}_2$ /NiMoAl coatings with the cavitation erosion data given in the literature [18,19,24,25].

**Table 2.** Reference samples used in cavitation erosion tests.

Sample Code	Grade	Main Chemical Element Composition (wt %)
AlSi	AlSi7Mg	Al base; Si 7.5%; Mg 6.5%
CuZn	CuZn40Pb2	Cu base; Zn 40%; Pb 2%
FeC	C45	Fe base; C 0.45%

The cavitation tests were conducted on an ultrasonic test stand, using the apparatus conforming to the ASTM G-32 [26] standard recommendations, according to an alternative stationary specimen method which is specifically for coatings testing. The gap between horn tip and test surface was set equal to 1 mm, and the amplitude and frequency of the tests were 50  $\mu\text{m}$  and 20 kHz, respectively. Distilled water was used as a cavitation test medium. The water temperature was stabilised at 25 °C. The tip diameter of the titanium sonotrode was 22 mm. The specimens with dimensions  $\varnothing 25 \times 5$  mm were machined from sprayed cylinders. The weights of the samples were measured before and during the test at regular intervals in order to determine cavitation erosion curves. The weight decrease of the samples was measured at specified time intervals with a 0.1 mg accuracy balance. After 15 min of cavitation, normalised cavitation erosion wear ( $Ne$ ) was calculated by dividing the measured volume loss of reference material by the volume loss of the coated samples, both tested under the same test conditions. The reference bulk metal alloy surfaces were prepared with the  $R_a$  roughness parameter lower than 0.08  $\mu\text{m}$ , and the coated specimens were investigated in as-sprayed conditions.

The cavitation-worn surface of the samples was assessed during time intervals of the cavitation test with SEM-EDS and optical microscopy using a stereoscope microscope Nikon SMZ 1500. Results of coating microstructural analysis and systematic cavitation-worn surface observations led to the elaboration of an innovative phenomenological model of cavitation erosion for  $\text{Al}_2\text{O}_3$ -40% $\text{TiO}_2$ /NiMoAl composite coatings.

## 3. Results and Discussion

### 3.1. Microstructure and Properties

The literature survey offers data about the properties of  $\text{Al}_2\text{O}_3$ - $\text{TiO}_2$  sprayed top coatings. However, there are very few studies providing information about composite coatings deposited by LVOF spraying with the blend of  $\text{Al}_2\text{O}_3$ -40% $\text{TiO}_2$  and NiMoAl powders [15]. In the present study, manufactured composite  $\text{Al}_2\text{O}_3$ -40% $\text{TiO}_2$ /NiMoAl coating morphology was investigated in cross section and on the surface of coatings (Figures 2 and 3, respectively). The general microstructure of a cermet coating is presented in Figure 2. The coating consists of a bonding layer (metallic) and a cermet layer (metallic-ceramic) which is deposited with different blends of ceramic and metallic powders. The bonding layer acts as a buffer to reduce the thermal stress originating during cooling of the sprayed coating to ambient temperature. The coating structures differ with respect to the amount of ceramic splats. It is visible in the microstructure cross section (Figure 2) and the coating surfaces

(Figure 3) that the amounts of ceramic lamellas and splats increase with the increase of cp portion ranging from 10% cp to 100% cp.

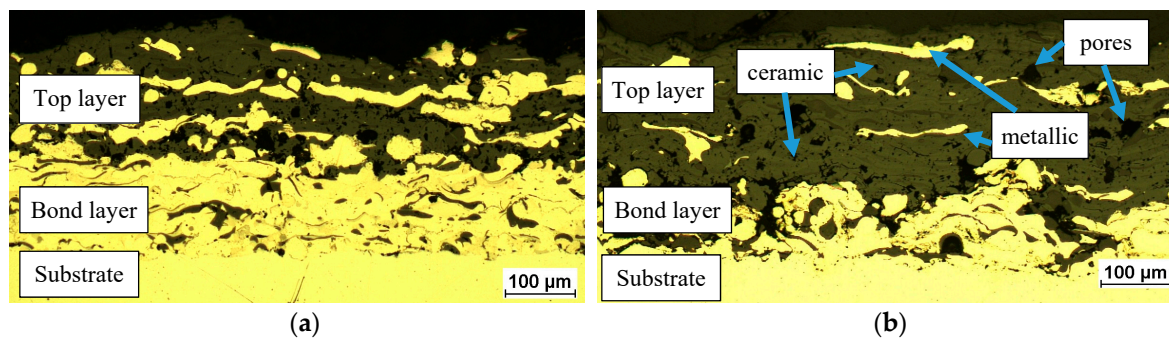


**Figure 2.** Microstructure of coatings deposited with the addition of (a) 50% cp and (b) 80% cp (ceramic powder)

The two-phase cermet top layer consists of ceramic and metallic lamellas derived from ceramic  $\text{Al}_2\text{O}_3\text{-40\%TiO}_2$  and metallic NiMoAl feedstock powders. Based on the microscopic observations shown in Figures 2 and 3, it is possible to indicate a typical lamellar microstructure of sprayed coatings [12,27] consisting of metal oxide particles, porosity, and partly melted or unmelted particles, which results in an uneven surface with microcracks in the ceramic phase. This network of microcracks is caused by the quenching stresses during the cooling of the ceramic lamella. Cracks in the ceramic phase are an inherent phenomenon occurring for the LVOF deposition of ceramic particles [4]. However, the coating cross section shows no presence of cracks penetrating through the coating thickness, which could negatively influence the coating wear resistance properties. Results of the chemical composition spot analysis (Figure 3) reveals that the brighter splats were sprayed with the metallic powder and mainly contain Ni and Al, Mo, O, and Ti. On the other hand, the darker splats contain chemical elements such as Ti, Al, and O and were made of the  $\text{Al}_2\text{O}_3\text{-40\%TiO}_2$  ceramic powder. A morphology analysis indicates that the ceramic lamellas are much more rounded and less flattened than the metallic lamellas which can be explained by the differences in their melting points.

The manufactured composite coatings have a relatively coarse structure (lamella interfaces are clearly visible), which is typical of LVOF-sprayed coatings. The examined microstructure exhibits much more rounded and larger pores as compared with the microstructure observed for the coatings prepared by the PS or HVOF methods, as described in [12,14]. This is connected with the impact energies of sprayed particles and process temperatures which are considerably different for LVOF spraying than for PS and HVOF processes.

The relationship between porosity and the  $\text{Al}_2\text{O}_3\text{-40\%TiO}_2$  feedstock powder composition was studied (Figure 4). Porosity measurements demonstrated that the average porosities of all coatings, except for those with 90% cp and 100% cp, were in the range of 9.8% to 10.8%, while the porosities of coatings with 90% cp and 100% cp were 11.6% and 13.3%, respectively. A denser structure was observed for the 40% cp and 50% cp cermet coatings. In general, the coatings have a relatively high porosity, which is in agreement with the literature of the subject. The porosity of LVOF-sprayed coatings is usually higher than that of PS or HVOF coatings [4,8]. However, relatively high porosity improves fracture toughness and allows the coating to alleviate internal stresses [3], which can have a beneficial effect on cavitation erosion resistance.

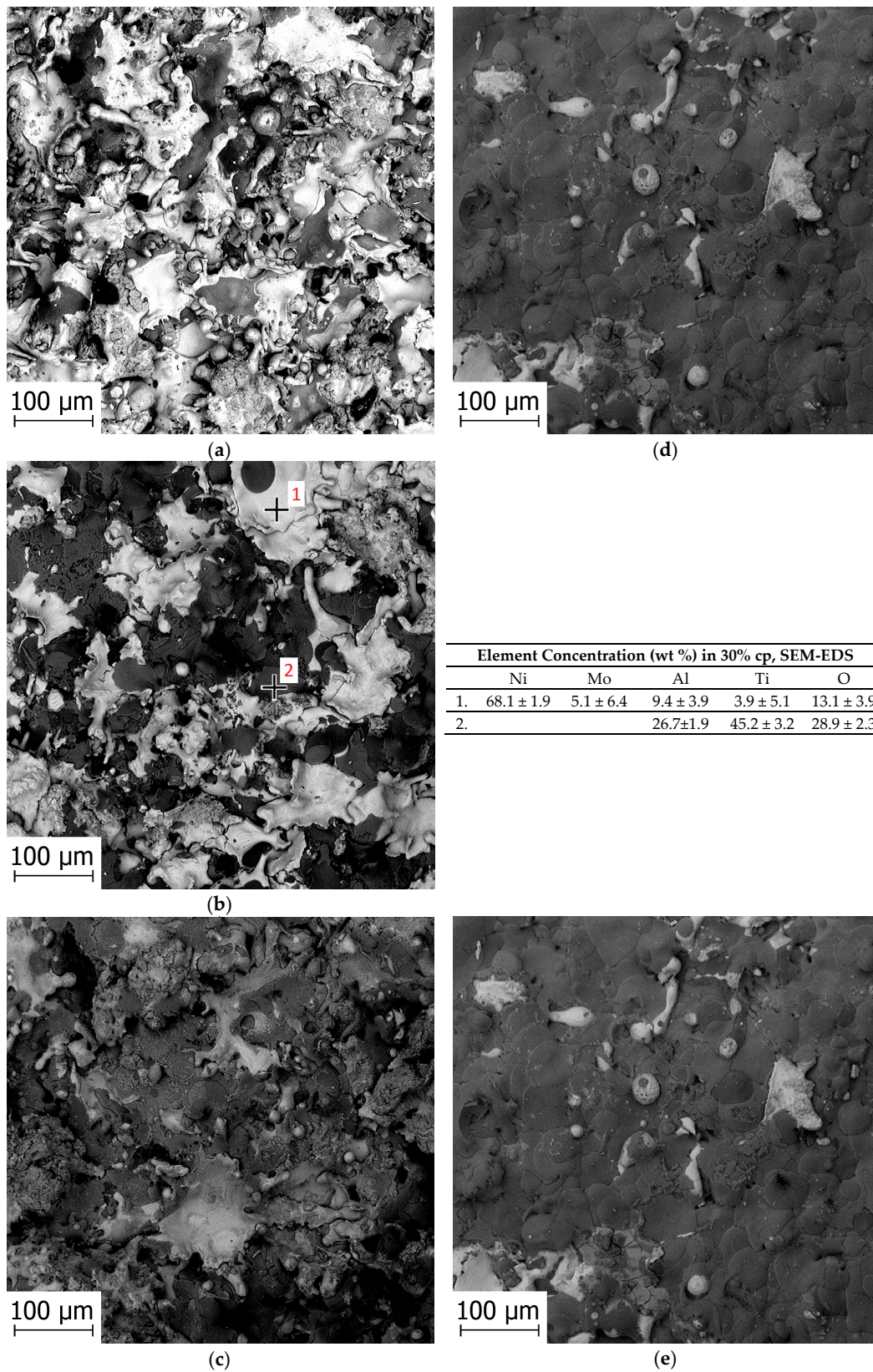


**Figure 3.** SEM images of as-sprayed coatings with (a) 0% cp, (b) 30% cp, (c) 60% cp, (d) 80% cp, and (e) 100% cp at high magnification, and the results of 30% cp sputers chemical analysis via SEM-EDS.

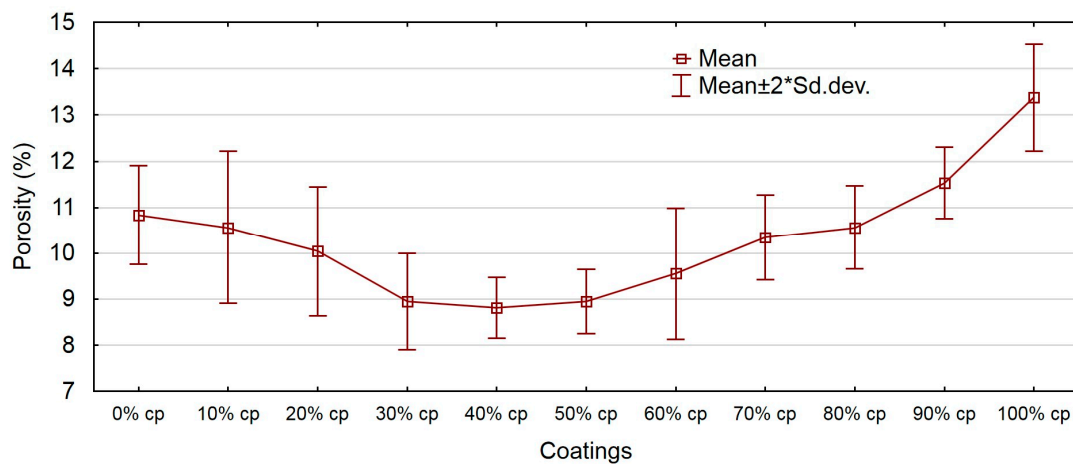


**Figure 4.** Influence of the ceramic powder (cp) content on coating porosity.

The as-sprayed coating surface roughness is attributed to the presence of lamellar structure, the unmelted particles, and the overlapping of splats and it derives from spraying parameters and ceramic-to-metallic-powder ratios. Metallic bond layer (0% cp) and 100% ceramic coating were sprayed with the parameters appropriate for metallic and ceramic powders, respectively. Cermet coatings were deposited using the parameters appropriate for ceramic powder to achieve melting of both metallic and ceramic materials. The surface roughness,  $R_a$ , of the as-sprayed cermet coatings ranges from 23.4  $\mu\text{m}$  to 28.2  $\mu\text{m}$ , while the  $R_a$  values of the 0% cp metallic bond coat and the ceramic top coating with 100% cp amount to 17.5  $\mu\text{m}$  and 18.8  $\mu\text{m}$ , respectively. High surface roughness of the cermet coating can be related to the differences in the particle sizes of metallic and ceramic feedstock powders, differences in the thermophysical properties of metallic and ceramic splats, and poor adhesion of ceramic to metallic splats. It can be seen in Figures 3 and 5 that the morphology of the as-sprayed coating develops according to the changes of ceramic feedstock powder composition. The  $R_a$  roughness parameter increases until the 50% cp content in the sprayed powder mixtures (Figure 5) and then decreases with further increase of cp content. Moreover, the  $R_a$  value of the as-sprayed coating with 100% cp feedstock powder is comparable with the same type of top-layer coating studied by Mishra et al. [2], which confirms that the spraying parameters of 100% cp were correct.

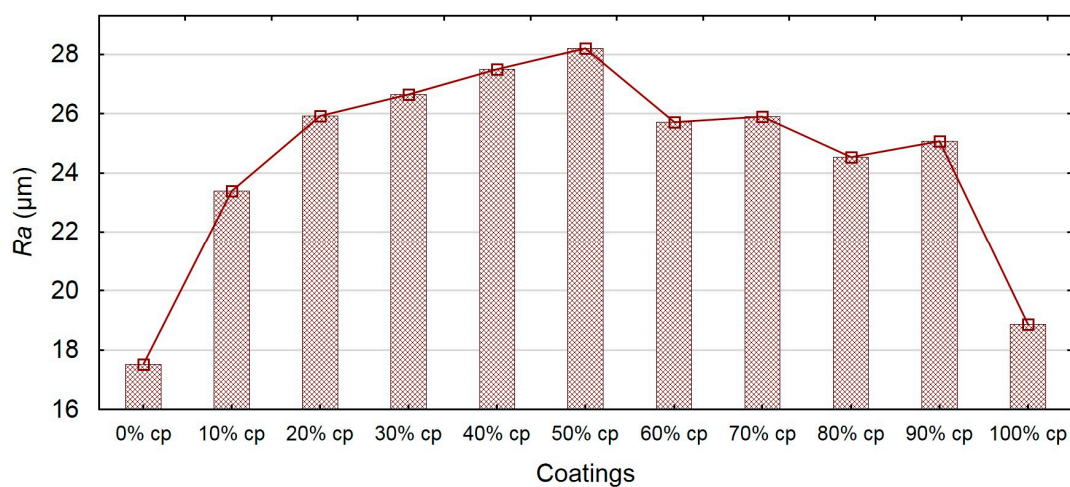


**Figure 5.** Effect of ceramic powder (cp) content on coating surface roughness.

The XRD patterns of the bond layer (100% mp), cermet top layer (blend containing 50% mp and 50% cp), and ceramic top layer sprayed with cp only are shown in Figure 6. The examination of the

XRD spectra revealed that the bond coat is composed of nickel solid solution and nickel oxide, while the coating produced with 100% cp consists of the aluminium titanate ( $\text{Al}_2\text{TiO}_5$ ) phase. The cermet coating sprayed with 50%  $\text{Al}_2\text{O}_3$ -40% $\text{TiO}_2$  is composed of the nickel solid solution and the  $\text{Al}_2\text{TiO}_5$  phase. In the spectra, phases such as rutile ( $\text{TiO}_2$ ) and  $\text{Al}_2\text{O}_3$  were not found.  $\text{TiO}_2$  melts at a lower temperature (1854 °C) than  $\text{Al}_2\text{O}_3$  (2040 °C) [28], and the presence of  $\gamma$ - $\text{Al}_2\text{O}_3$  in the coating was suggested by Mishra et al. [9]. However, the subsequent decomposition of  $\text{Al}_2\text{TiO}_5$  into rutile ( $\text{TiO}_2$ ) and  $\text{Al}_2\text{O}_3$  is possible at high temperatures of >1280 °C [3] and takes place e.g., in the diesel engine, as discussed in [16].

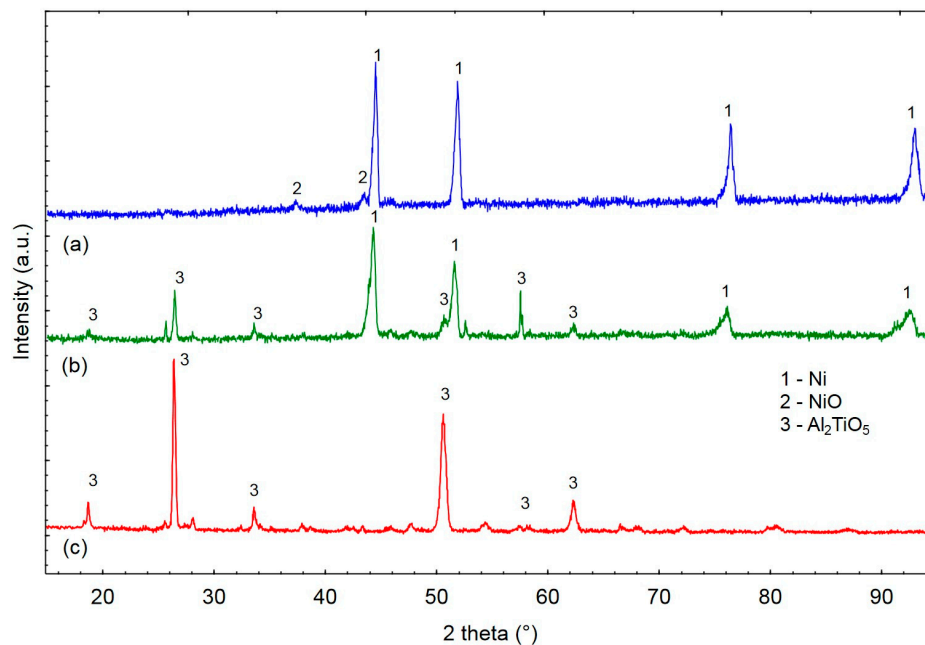


**Figure 6.** XRD pattern of as-sprayed (a) bond layer, (b) coating with 50% cp, and (c) coating sprayed with 100% ceramic powder.

The results of the hardness and Young's modulus examination of the main cermet coating phases are presented in Table 3. The hardness of the ceramic phase is more than two times higher than that of the metallic phase, in contrast to the Young modulus value that is slightly lower for the ceramic phase. The results of hardness and Young's modulus indicate that the ceramic lamellas are more brittle than metallic ones. The results presented in Table 3 are in line with previous findings of the authors [15]. The hardness is in the range of hardness values presented in [2] for the LVOF-sprayed  $\text{Al}_2\text{O}_3$ -40% $\text{TiO}_2$  coatings, but is lower than that of PS [10,11] or HVOF [12]  $\text{Al}_2\text{O}_3$ - $\text{TiO}_2$  coatings. The relatively high value for the standard deviation of hardness values demonstrates that the coating microstructure incorporates porosity, voids, and defects formed by partially melted or unmelted powder particles, which is in agreement with metallographic results. Also, the hardness value spread for the LVOF coatings is clearly wider than that obtained for the PS coatings, which results from a less dense structure of the coatings deposited by the LVOF than those produced by the HVOF or PS processes.

**Table 3.** Mechanical properties of the coatings.

Microstructure Phase	Nanohardness (HV)		Young's Modulus (GPa)	
	Average	SD	Average	SD
ceramic lamellas	723.2	310.7	110.4	20.2
metallic lamellas	325.5	40.8	116.8	23.1

### 3.2. Cavitation Erosion

The results of the cavitation erosion investigation are presented in Figures 7–15. The ultrasonic test stand used in our study generates intensive cavitation in comparison to cavitation tunnel with system of barricades or cavitation jet cell testing equipment [24]. Thus, the effect of the cavitation wear of sprayed coatings was determined in a relatively short period of time, in contrast to that observed for the reference bulk alloys. In the cavitation erosion process, the acceleration and deceleration stages of erosion can be distinguished. These stages occur especially during the testing of metal alloy samples according to ASTM G-32, with the incubation stage easily distinguishable [26,29,30]. On the other hand, the process of ceramic material wear differs from that observed for metal alloys. The initial stage of cavitation erosion of ceramic samples can be very short, as reported for alumina in [31].

The analysis of the cavitation erosion curves (Figure 7) of the tested sprayed  $\text{Al}_2\text{O}_3$ -40% $\text{TiO}_2$ /NiMoAl coatings reveals that the incubation stage is negligible. In addition, the mass loss rate is constant for every tested cermet coating, as opposed to the AlSi metal alloy. Jafarzadeh and Ghavidel [10] observed a similar effect for plasma-sprayed  $\text{Al}_2\text{O}_3$ -13% $\text{TiO}_2$  coatings; however, they did not test any reference material, and, therefore, a comparison of the results is difficult. In our study, the cermet coatings and metal alloys (structural steel FeC, brass CuZn, and cast aluminium alloy AlSi) were tested in similar test conditions. Apart from the AlSi sample, the FeC and CuZn metal alloy samples showed negligible mass loss after the test time. The surfaces of cavitation-worn reference samples are shown in Figure 8.

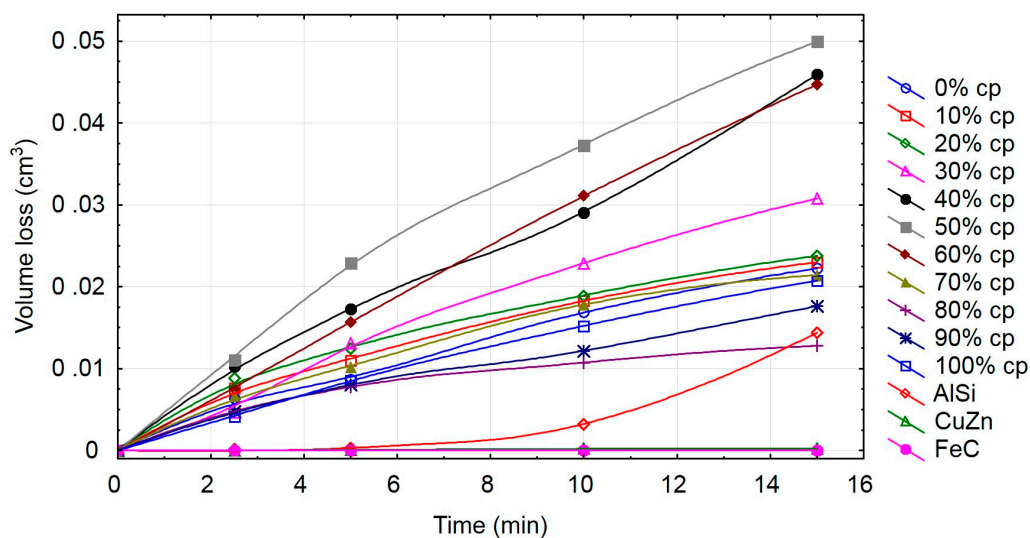


Figure 7. Cumulative erosion–time curves for the tested coatings.

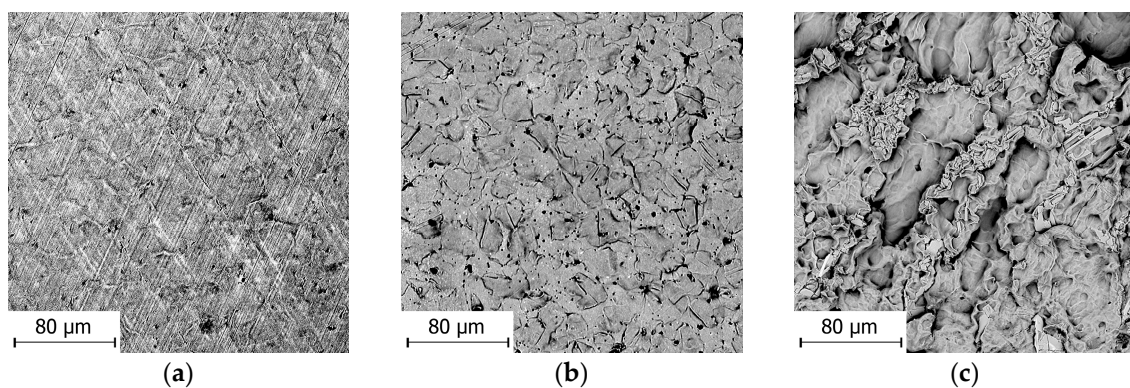


Figure 8. Cavitation-worn surface of metal samples, SEM: (a) FeC (15 min), (b) CuZn (15 min), (c) AlSi (5 min).

Cavitation erosion is a fatigue process. After the cavitation erosion incubation period, specific for each metal alloy, material loss occurs and pits start to develop on its surface. The wear of metal alloys usually starts with plastic deformation of metal grains due to hydrodynamic cavitation. After 15 min of cavitation, the FeC samples (Figure 8a) show changes in their surface topography. The surface of the CuZn sample (Figure 8b) is also deformed and some pits are visible; however, the mass loss is within the range of measurement error. On the other hand, AlSi exhibits a heavily eroded surface (Figure 8c) and material loss (Figure 7). The analysis of the cavitation erosion curves and damaged surfaces of the reference samples (Figures 7 and 8) allows us to state that the tested aluminium alloy exhibits an accelerated stage of erosion, while the FeC and CuZn samples show an incubation period of cavitation. The wear mechanism of AlSi was discussed in detail in our previous work [29]. It is known that the fine grain structure of wrought metal alloys has a beneficial influence on their resistance to cavitation erosion. AlSi has a typical as-cast coarse dendritic structure, which accelerates cavitation erosion. AlSi is less resistant to cavitation erosion than FeC and CuZn specimens. Thus, the normalised erosion resistance of coatings was calculated in relation to the AlSi sample, presented in Figure 9. The cermet  $\text{Al}_2\text{O}_3$ -40% $\text{TiO}_2$ /NiMoAl coating exhibits a relatively low resistance to cavitation. The lowest resistance to cavitation was identified for the coating with 50% cp, for which the normalized erosion resistance equals 0.29, which is four times lower than the highest cavitation resistance observed for the coating containing 80% cp. Therefore, 80% of  $\text{Al}_2\text{O}_3$ -40% $\text{TiO}_2$  in feedstock powder seems optimal for this type of cermet coating (Figures 9 and 10). The mass content of  $\text{Al}_2\text{O}_3$ -40% $\text{TiO}_2$  in  $\text{Al}_2\text{O}_3$ -40% $\text{TiO}_2$  /NiMoAl mixture feedstock powders influences the cermet roughness and porosity, and, as a result, its cavitation erosion resistance (Figures 11 and 12).

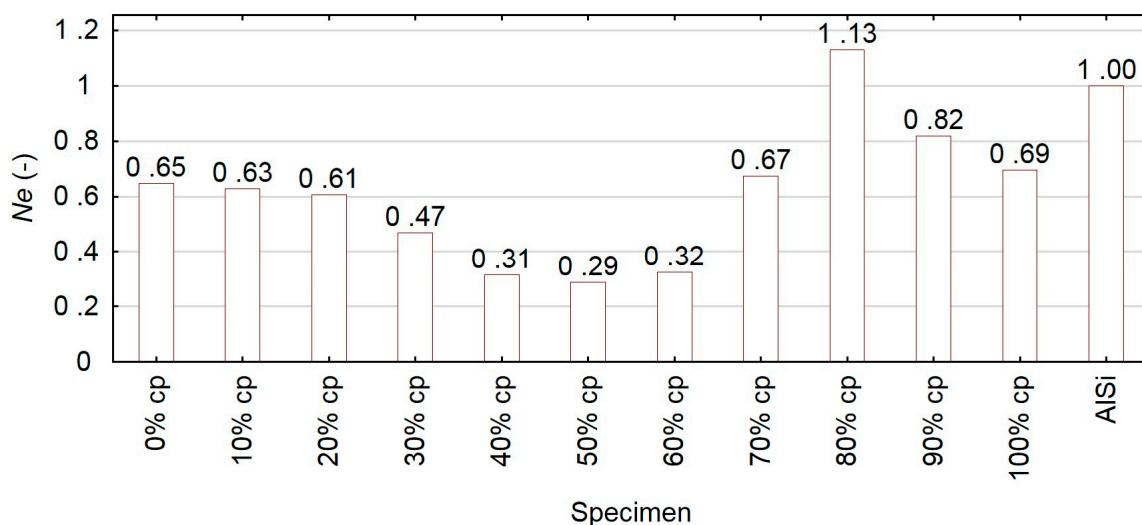


Figure 9. Normalized cavitation erosion resistance ( $N_e$ ) of the coatings.

Although no strong correlation was found, we claim that the coating roughness and porosity affect its cavitation erosion resistance (Figures 11 and 12). Generally, with increased cermet coating roughness we observe a decrease in the cavitation erosion resistance (Figure 11). On the other hand, the increase in porosity has a positive effect on the coating cavitation erosion resistance (Figure 12). This agrees with Cui et al. [3], who observed that the high coating porosity improves fracture toughness and alleviates coating internal stresses [3], which can have a positive effect on the cavitation erosion resistance of cermet coatings.

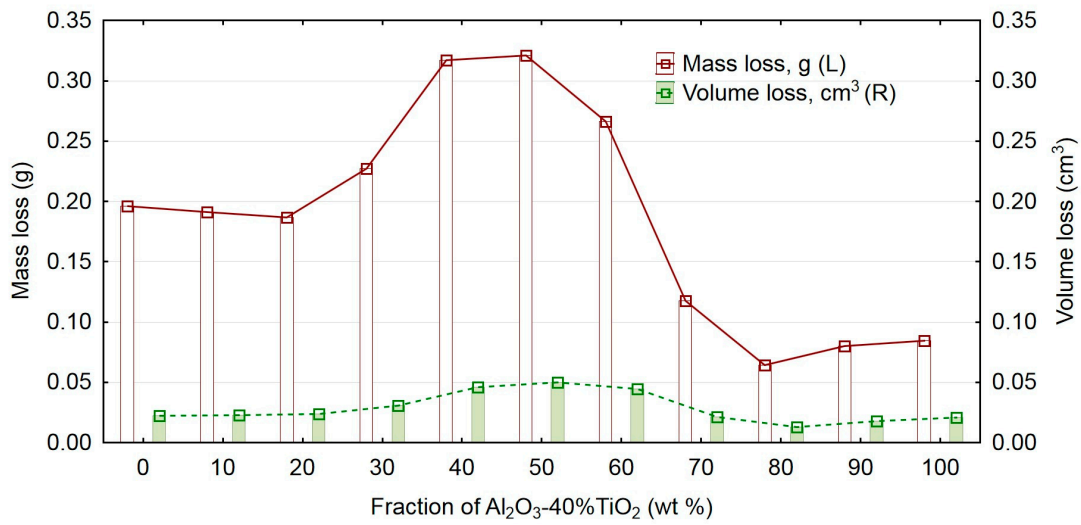


Figure 10. Influence of  $\text{Al}_2\text{O}_3\text{-40\%TiO}_2$  content on coating material loss.

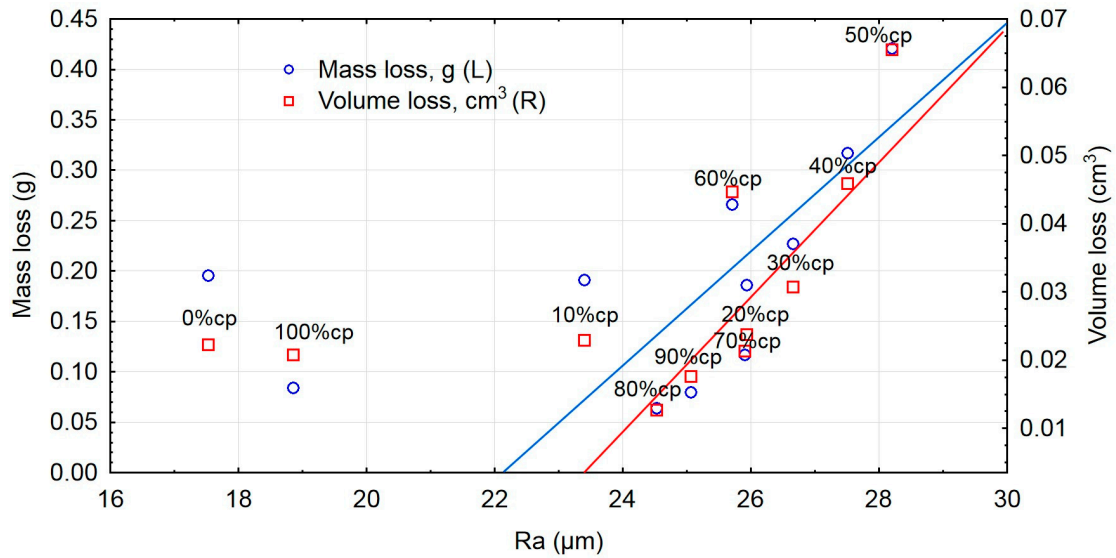


Figure 11. Influence of coating roughness on its mass and volume loss after 15 min of cavitation testing.

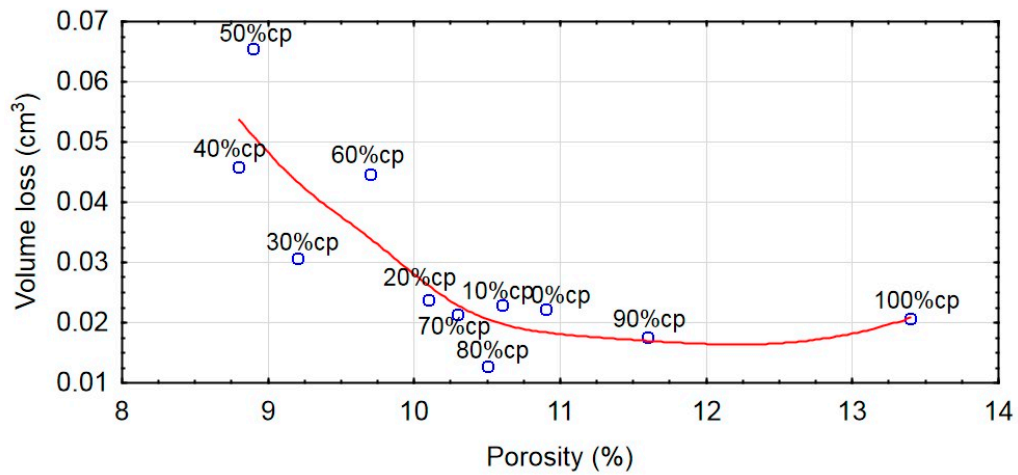
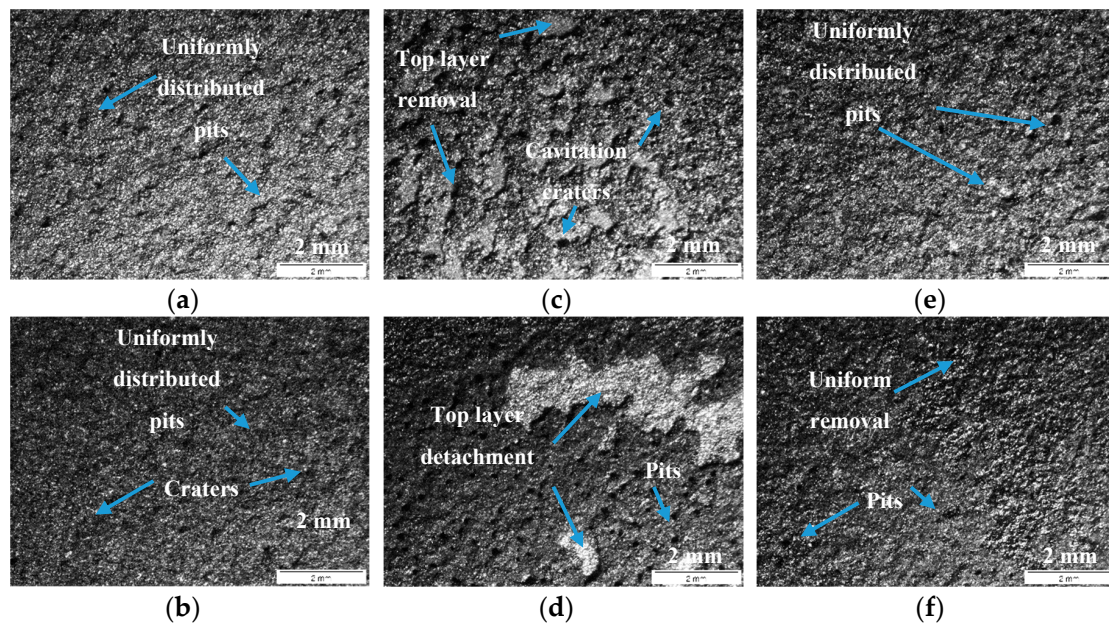


Figure 12. Effect of coating porosity on cumulative volume loss.

### 3.3. Cavitation Erosion Mechanism and the Phenomenological Model of $\text{Al}_2\text{O}_3$ -40% $\text{TiO}_2$ /NiMoAl Coatings

The cavitation erosion mechanism of  $\text{Al}_2\text{O}_3$ -40% $\text{TiO}_2$ /NiMoAl coatings is investigated based on systematic SEM-EDS and LOM observations, and the results of investigations are shown in Figures 13–15. The progress of cermet coating erosion was analysed by comparing the as-sprayed coatings (shown in Figure 3) with those subjected to cavitation tests (Figures 13 and 14). The progress of cermet coating cavitation erosion was analysed based on observations conducted at different time intervals (Figure 15). Based on that, a phenomenological model of  $\text{Al}_2\text{O}_3$ -40% $\text{TiO}_2$ /NiMoAl cermet cavitation erosion was elaborated (see Figure 16).



**Figure 13.** Cavitation-worn surfaces of  $\text{Al}_2\text{O}_3$ -40% $\text{TiO}_2$ /NiMoAl cermet coatings deposited with (a) 10% cp, (b) 20% cp, (c) 40% cp, (d) 50% cp, (e) 80% cp and (f) 90% cp ceramic powder contents % cp; LOM, stereoscope microscope.

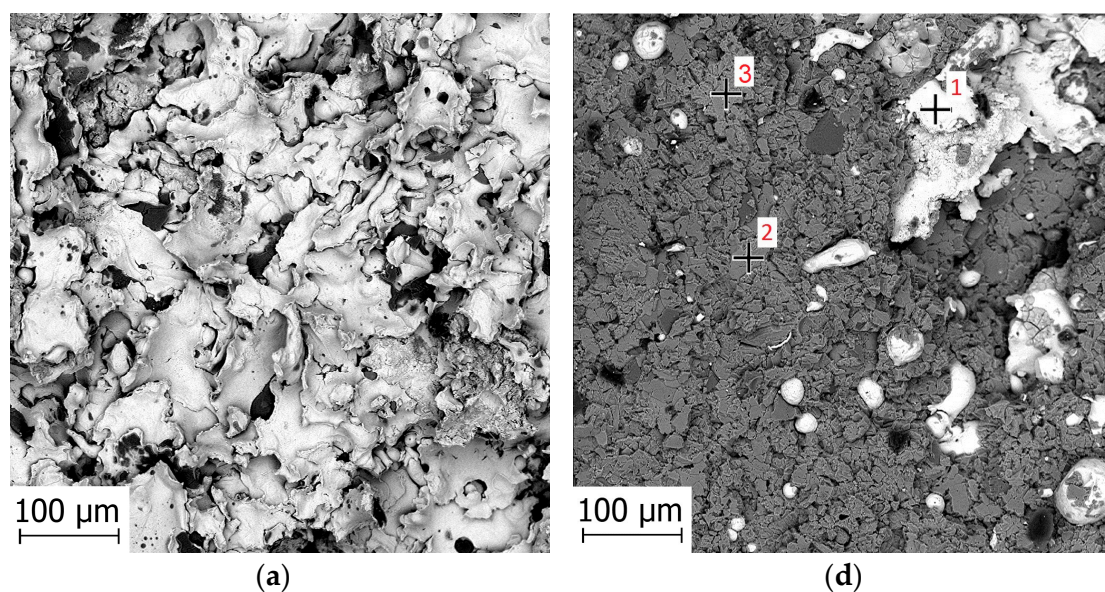


**Figure 14.** Cont.

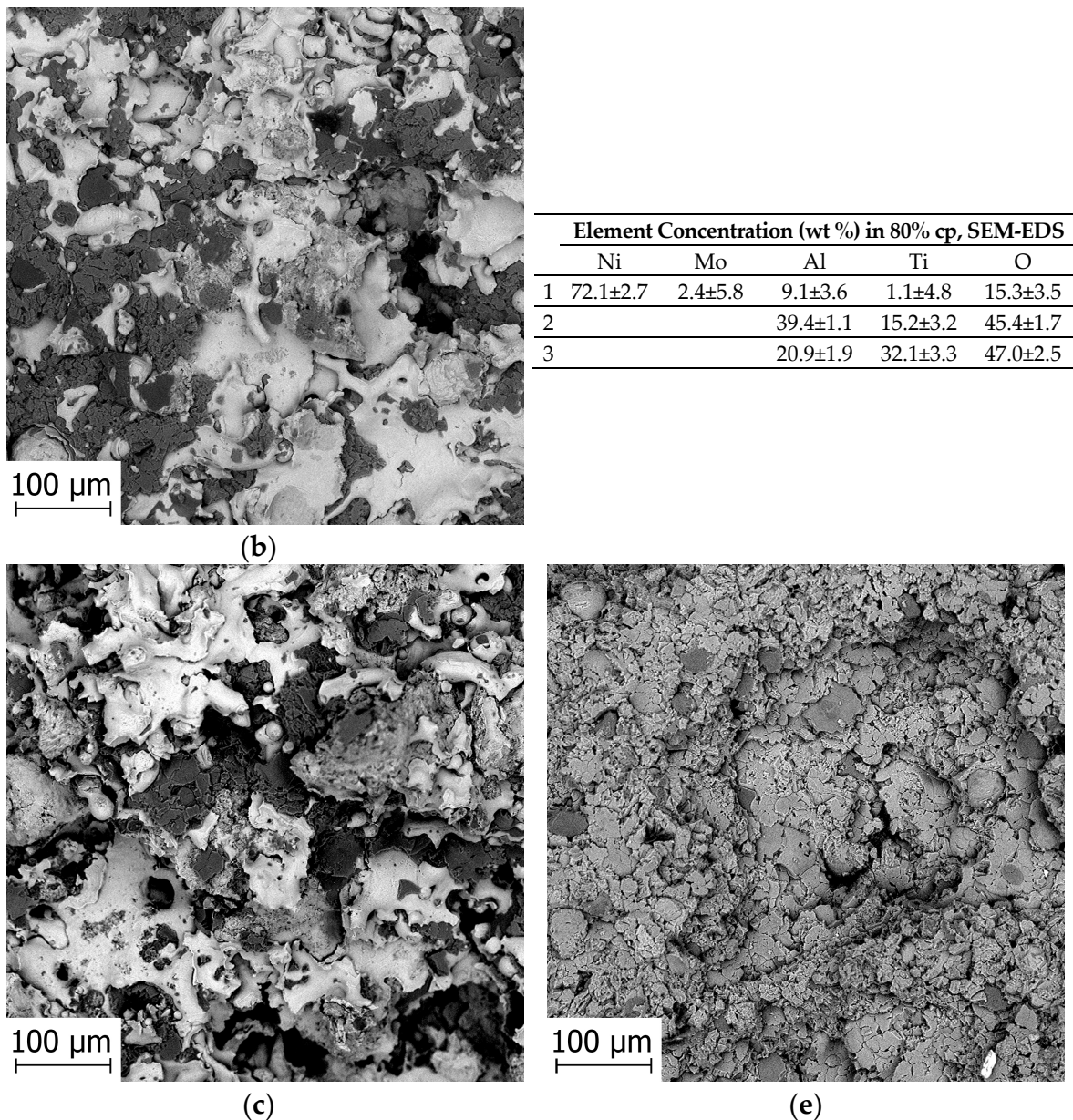


**Figure 14.** Coatings after 15 min of cavitation (a) 0% cp, (b) 30% cp, (c) 60% cp, (d) 80% cp, and (e) 100% cp (SEM) and results of 80% cp spot chemical analysis (SEM-EDS). Worn surfaces of coatings correspond to the as-sprayed surfaces shown in Figure 3.

The effect of the cp content on the erosion of coatings was studied on the basis of macroscopic (Figure 13) and microscopic (Figure 14) observations. The erosion of cermet  $\text{Al}_2\text{O}_3$ -40% $\text{TiO}_2$ /NiMoAl coatings deposited with 10–30% cp and 70–90% cp proceeds at an almost constant rate with a uniform pit distribution, whereas the erosion of coatings produced with 40–60% cp consists of the removal of massive chunks of material and the formation of craters, as shown in Figure 13. After 15 min of testing, huge pits in the coating were identified and the bond coat was exposed (Figures 13 and 14). The CERs of the samples produced with the highest contents of powders are at a similar level, as confirmed by the plot in Figure 10. The mass losses in the coatings mainly composed of metallic feedstock powder with the addition of 10% to 30% cp are similar (Figure 10). Similar results can be observed for the coatings sprayed with a high content of ceramic with 80% to 100% cp. The erosion patterns of coatings with a higher content of ceramic phase are more uniform compared with those of coatings rich in metallic phase (Figures 13 and 14). It seems that the differences between the metallic

and ceramic lamella properties such as hardness and Young's modulus (Table 3) affect the cavitation erosion process of cermet  $\text{Al}_2\text{O}_3$ -40% $\text{TiO}_2$ /NiMoAl coatings. The conducted investigations reveal that the hard and brittle  $\text{Al}_2\text{O}_3$ - $\text{TiO}_2$  phase is more susceptible to cavitation erosion than NiMoAl splats, and, thus, the cermet erosion starts in ceramic lamellas (Figure 14). The addition of 20% of NiMoAl feedstock powder prevents the ceramic phases from detaching in massive chunks. Summing up, we maintain that an 80% proportion of  $\text{Al}_2\text{O}_3$ -40% $\text{TiO}_2$  in an  $\text{Al}_2\text{O}_3$ -40% $\text{TiO}_2$ /NiMoAl mixture is optimal for the cavitation erosion resistance of cermet coatings.

The observations conducted at higher magnification (Figure 15) allow to formulate the general model of cavitation erosion of  $\text{Al}_2\text{O}_3$ -40% $\text{TiO}_2$ /NiMoAl. The heterogeneous structure of the LVOF thermally sprayed coatings consists of ceramic and metallic lamellas, partially melted or unmelted particles, lamella interfaces, porosity, and microcracks. It was demonstrated by the LOM, SEM, and EDS chemical analysis (Figures 2, 3 and 14) that the two main lamellas in the cermet structure are metallic (NiMoAl) and ceramic ( $\text{Al}_2\text{O}_3$ -40% $\text{TiO}_2$ ). The model of the cermet structure is presented in Figure 16a, and the mechanism of cavitation erosion is schematically depicted in Figure 16b,c.

The process of material removal from cermet coatings starts almost without the incubation period of cavitation erosion (see the plot in Figure 7). The first stage of erosion was the removal of splats with low coherence, then the edges of overlapping particles or loose splats were detached (see Figures 3 and 14). As mentioned before, coating morphology and roughness affect the cavitation erosion of cermet. The degradation of cermet structure mainly relies on the removal of ceramic  $\text{Al}_2\text{O}_3$ - $\text{TiO}_2$  lamellas, as shown in Figure 16b. It is demonstrated in Figure 15a,b that the structure inhomogeneity such as the presence of primary microcracks in ceramic lamellas plays a major role in the initiation of erosion, resulting in ceramic crushing and spalling. Ceramic splats have higher brittleness (Table 3) than metallic ones; thus, the identified cavitation erosion mechanism was brittle fracture (Figure 15c). These microcracks propagate through the ceramic lamellas and connect with voids, pits, and other cracks, consequently eliminating the ceramic phase from the cermet structure. The coating microstructure exhibits porosity, which also influences the cavitation wear of cermet (Figure 4). The erosion starts in the ceramic lamellas (Figure 15d) and continues by the removal of the exposed metallic splats and unmelted particles (see Figures 14 and 15a,b,e,g). Exposed to cavitation, metallic lamellas undergo cracking, as shown in Figure 15f,g,h. In particular, the edges of overlapping metallic splat lamellas undergo cavitation erosion and the whole unmelted particles are taken out (Figure 15d,e and Figure 16c). Then, the alternating removal of cermet structural components proceeds in the bond layer direction. Once the cracks connect with the pores, deep cavitation pits (craters) occur (Figure 15i,j and Figure 16c). Then, metallic lamellas lose support from ceramic and detach from the cermet. This results in cracking and the extraction of metallic lamellas, which consequently leads to metallic splat detachment, as shown in Figures 15f and 16d. The erosion process proceeds alternatively splat-by-splat, towards the bond layer (Figure 15g,h). Finally, severe erosion encompasses the entire cermet coating and large craters are formed (Figure 13), as shown in Figure 16d. The cavitation erosion of cermet coatings increases worn-surface roughness, which accelerates the damage of the coating material in the form of large blocky particles or the detachment of whole splats, as shown in Figure 13.

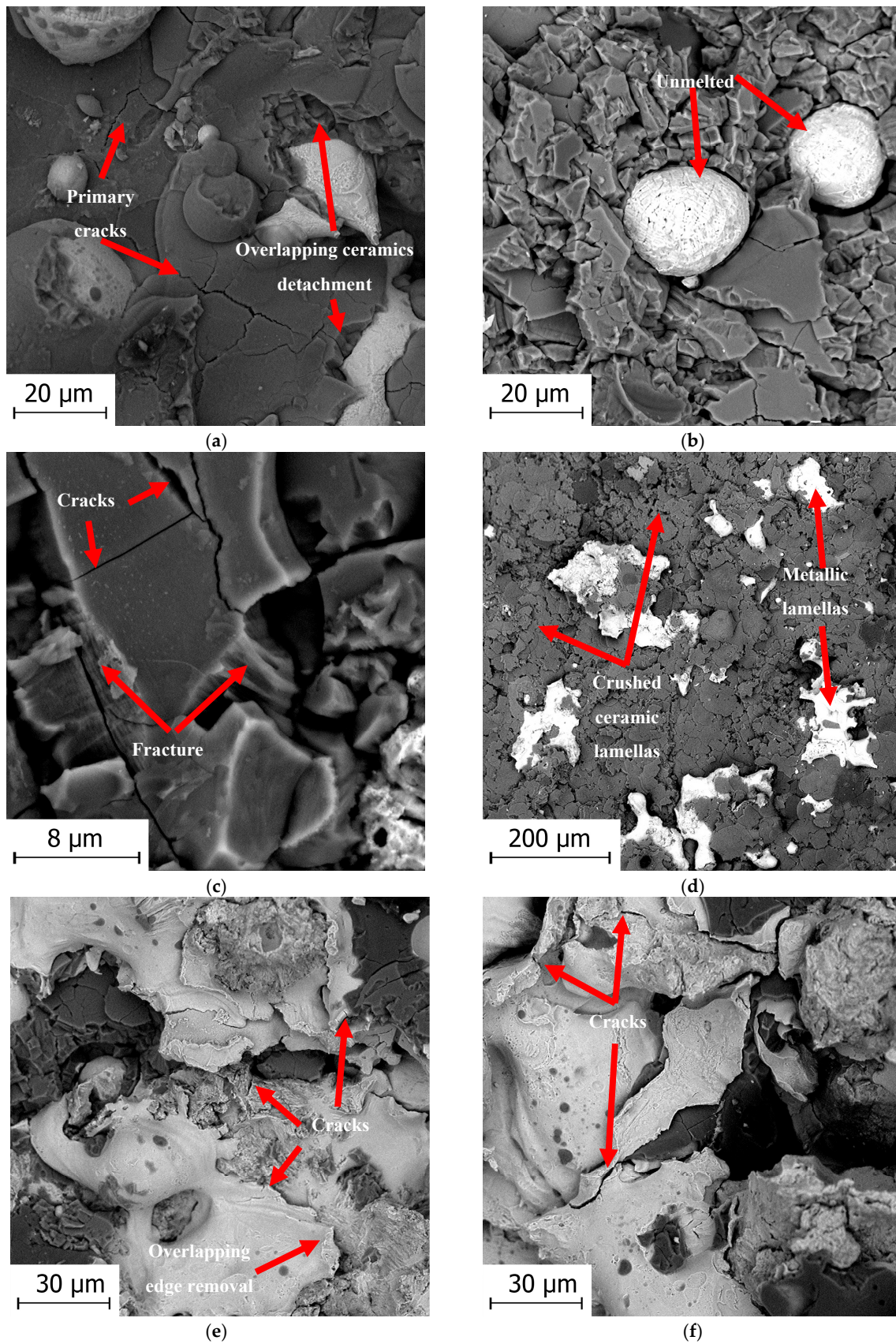
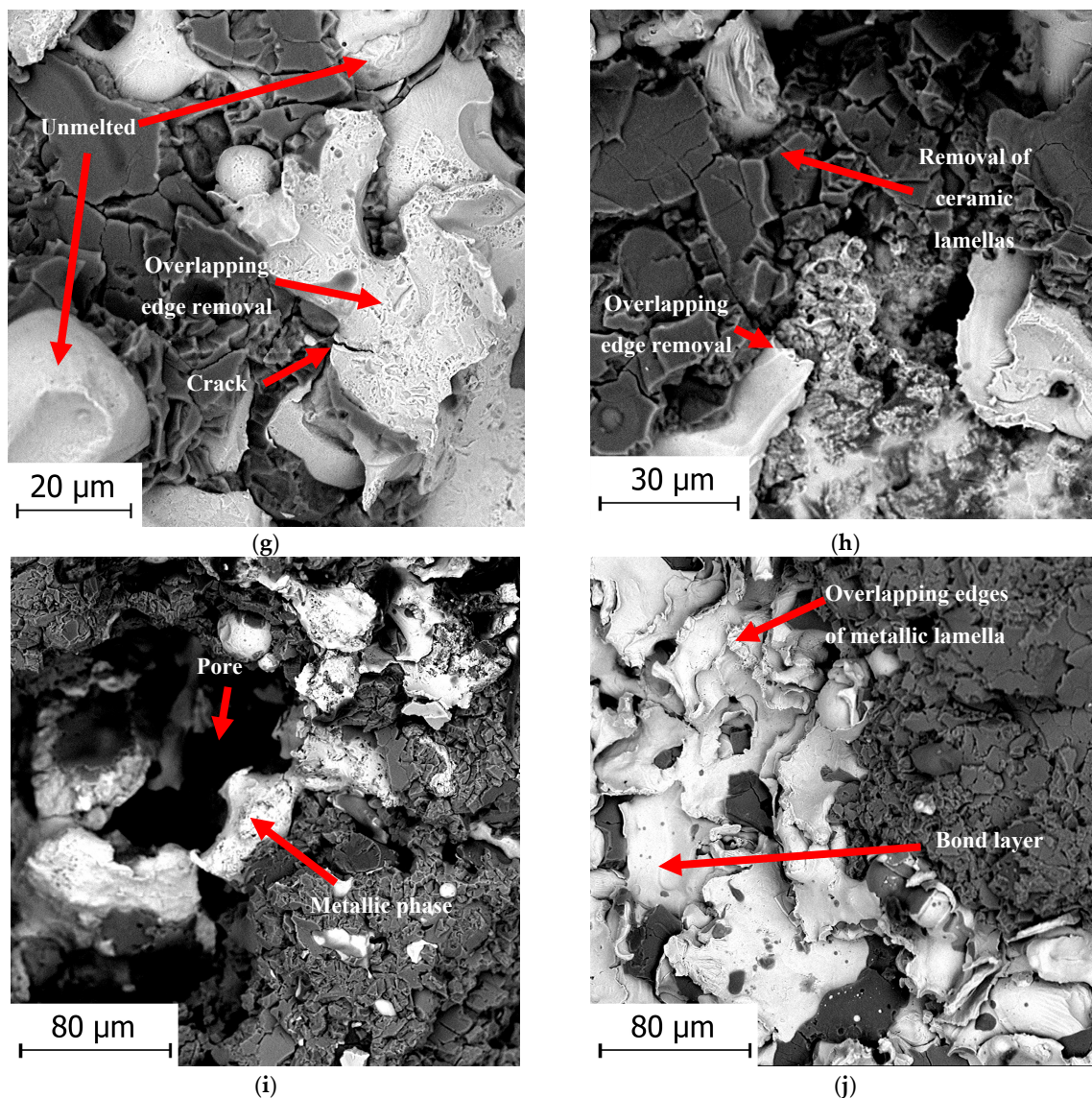
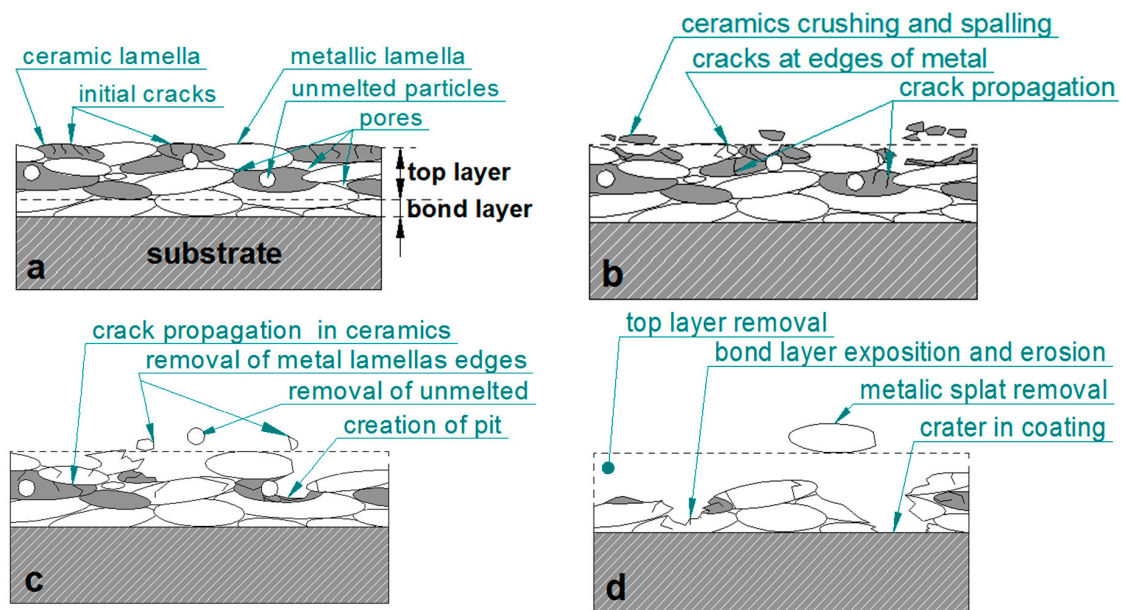


Figure 15. Cont.



**Figure 15.** Selected areas of cavitation-worn cermet coatings observed at different time intervals via SEM. (a) Initial cracks and removal of ceramics top of metallic splats, 80% cp, 5 min; (b) Fragmentation of ceramics and exposition of unmelted metallic particles, 80% cp, 10 min; (c) Brittle fracture and cracks in ceramic lamellas, 60% cp, 5 min; (d) Exposition of metallic splats due to ceramic removal, 90% cp, 10 min; (e) Detachment of overlapping metallic lamellas starting at the edges, 20% cp, 5 min; (f) Formation of cracks in exposed metallic phase, 40% cp, 10 min; (g) Removal of phases starting with the removal of ceramic and metallic splat edges, and the exposition of unmelted particles, 50% cp, 5 min; (h) Alternate removal of splats starting with the detachment of ceramic lamellas and metallic splat edges, 60% cp, 10 min; (i) Pit growth due to coating material removal and connection with inhomogeneity (pore), 50% cp, 10 min; (j) Edge of the crater, bond layer exposed. Detachment of overlapping metallic lamella, 70% cp, 15 min.



**Figure 16.** Phenomenological model of cermet coating cavitation erosion: (a) coating before cavitation; (b–d) successive changes in the coating due to cavitation erosion.

#### 4. Conclusions

In this study, cavitation wear testing of  $\text{Al}_2\text{O}_3$ -40% $\text{TiO}_2$ /NiMoAl cermet coatings deposited via an LVOF flame spray process onto steel substrates was performed. The cavitation erosion resistance and wear mechanism of the flame-sprayed  $\text{Al}_2\text{O}_3$ -40% $\text{TiO}_2$ /NiMoAl cermet coatings as well as the effect of feedstock powder ratios ( $\text{Al}_2\text{O}_3$ - $\text{TiO}_2$ /NiMoAl) of deposited cermet coatings on their cavitation erosion resistance were determined. General relationships between the properties, microstructure, and cavitation wear resistance of the coatings were examined and the following conclusions were drawn:

- Cermet coatings sprayed with the mixtures of  $\text{Al}_2\text{O}_3$ -40% $\text{TiO}_2$  and NiMoAl feedstock powders were successfully deposited by LVOF spray. The microstructure of sprayed cermet contained unmelted particles, ceramic and metallic lamellas, lamella interfaces, porosity, oxide particles, and microcracks. The average hardnesses of ceramic and metallic lamellas were 727 HV and 327 HV, respectively. The porosity was in the range of 9.8–13.3%. The surface roughness  $R_a$  of as-sprayed cermet ranged from 23.4  $\mu\text{m}$  to 28.2  $\mu\text{m}$ .
- The composition of the blend of the  $\text{Al}_2\text{O}_3$ -40% $\text{TiO}_2$  and NiMoAl feedstock powders affects the cavitation erosion resistance of cermet coatings. The coating sprayed with the mixture containing 80 wt % of  $\text{Al}_2\text{O}_3$ -40% $\text{TiO}_2$  exhibits a higher cavitation erosion resistance than other cermet.
- The cermet coating sprayed with the  $\text{Al}_2\text{O}_3$ -40% $\text{TiO}_2$ /NiMoAl mixture containing 80 wt % of  $\text{Al}_2\text{O}_3$ -40% $\text{TiO}_2$  has more than 10% higher normalised cavitation erosion resistance than the reference aluminium alloy. By contrast, the cavitation wear rates of the cermet coatings were higher than those of the reference steel and brass samples.
- The main difference in the cavitation erosion process of the coatings and metal alloys consists of the evident incubation stage of cavitation erosion identified for reference materials and negligible incubation period of cavitation erosion as well as constant erosion rate acknowledged for thermally sprayed coatings.
- Porosity and surface roughness affect cavitation erosion resistance (CER). Large porosity or/and small surface roughness have a positive effect on the CER of cermet coatings.
- The investigation revealed that the hard and brittle ceramic phase is more susceptible to cavitation erosion than are the metallic splats. The dominant mechanism of the cavitation erosion of composite coatings is brittle fracture initiated at primary microcracks present in ceramic lamellas,

which results in ceramic splat removal. Then, exposed to cavitation, the metallic lamellas undergo erosion and the overlapping edges of splats are prone to erosion.

- The phenomenological model of the cavitation erosion of the  $\text{Al}_2\text{O}_3$ -40% $\text{TiO}_2$ /NiMoAl cermet coatings was elaborated. The erosion of cermet coatings starts with the removal of ceramic lamellas. The cavitation erosion is accelerated by cermet structural nonuniformities or discontinuities in the cermet coating microstructure such as crack networks, unmelted particles, and porosity. The progress of erosion depends on the differences in the mechanical properties of ceramic and metallic lamellas. The study confirmed that any inhomogeneity such as primary microcracks in ceramic lamellas plays a major role in the initiation of erosion, which leads to ceramic crushing and spalling.

**Author Contributions:** Conceptualization, M.S. and T.H.; Methodology, M.S. and T.H.; Validation, M.S. and T.H.; Formal Analysis, M.S.; Investigation, M.S. and T.H.; Resources, T.H.; Visualization, M.S.; Writing-Original Draft Preparation, M.S.; Writing-Review & Editing, M.S. and T.H.

**Funding:** This research was funded by Lublin University of Technology, Poland grant number 20/MN/2017.

**Conflicts of Interest:** The authors declare no conflict of interest.

## References

1. Gao, X.; Tian, Z.; Liu, Z.; Shen, L. Interface characteristics of  $\text{Al}_2\text{O}_3$ -13% $\text{TiO}_2$  ceramic coatings prepared by laser cladding. *Trans. Nonferrous Met. Soc. China* **2012**, *22*, 2498–2503. [[CrossRef](#)]
2. Mishra, N.K.; Mishra, S.B. Hot corrosion performance of LVOF sprayed  $\text{Al}_2\text{O}_3$ -40%  $\text{TiO}_2$  coating on Superni 601 and Superc 605 superalloys at 800 and 900°C. *Bull. Mater. Sci.* **2015**, *38*, 1679–1685. [[CrossRef](#)]
3. Cui, S.; Miao, Q.; Liang, W.; Zhang, Z.; Xu, Y.; Ren, B. Tribological Behavior of Plasma-Sprayed  $\text{Al}_2\text{O}_3$ -20 wt.% $\text{TiO}_2$  Coating. *J. Mater. Eng. Perform.* **2017**, *26*, 2086–2094. [[CrossRef](#)]
4. Davis, J.R. *Handbook of Thermal Spray Technology*; ASM International: Geauga County, OH, USA, 2004; ISBN 978-0-87170-795-6.
5. Czupryński, A. Selected Properties of Thermally Sprayed Oxide Ceramic Coatings. *Adv. Mater. Sci.* **2015**, *15*, 17–32. [[CrossRef](#)]
6. Szymański, K.; Hernas, A.; Moskal, G.; Myalska, H. Thermally sprayed coatings resistant to erosion and corrosion for power plant boilers—A review. *Surf. Coat. Technol.* **2015**, *268*, 153–164. [[CrossRef](#)]
7. Yao, Y.; Lyckfeldt, O.; Tricoire, A.; Tricoire, A. Microstructure of Plasma Sprayed  $\text{Al}_2\text{O}_3$ -3wt% $\text{TiO}_2$  Coating Using Freeze Granulated Powder. *J. Mater. Sci. Chem. Eng.* **2016**, *04*, 8. [[CrossRef](#)]
8. Jia, S.; Zou, Y.; Xu, J.; Wang, J.; Yu, L. Effect of  $\text{TiO}_2$  content on properties of  $\text{Al}_2\text{O}_3$  thermal barrier coatings by plasma spraying. *Trans. Nonferrous Met. Soc. China* **2015**, *25*, 175–183. [[CrossRef](#)]
9. Mishra, N.K.; Mishra, S.B.; Kumar, R. Oxidation resistance of low-velocity oxy fuel-sprayed  $\text{Al}_2\text{O}_3$ -13% $\text{TiO}_2$  coating on nickel-based superalloys at 800°C. *Surf. Coat. Technol.* **2014**, *260*, 23–27. [[CrossRef](#)]
10. Jafarzadeh, K.; Valefi, Z.; Ghavidel, B. The effect of plasma spray parameters on the cavitation erosion of  $\text{Al}_2\text{O}_3$ - $\text{TiO}_2$  coatings. *Surf. Coat. Technol.* **2010**, *205*, 1850–1855. [[CrossRef](#)]
11. Morks, M.F.; Akimoto, K. The role of nozzle diameter on the microstructure and abrasion wear resistance of plasma sprayed composite coatings. *J. Manuf. Process.* **2008**, *10*, 1–5. [[CrossRef](#)]
12. Matikainen, V.; Niemi, K.; Koivuluoto, H.; Vuoristo, P. Abrasion, Erosion and Cavitation Erosion Wear Properties of Thermally Sprayed Alumina Based Coatings. *Coatings* **2014**, *4*, 18–36. [[CrossRef](#)]
13. Żórawski, W.; Góral, A.; Bokuvka, O.; Lityńska-Dobrzyńska, L.; Berent, K. Microstructure and tribological properties of nanostructured and conventional plasma sprayed alumina–titania coatings. *Surf. Coat. Technol.* **2015**, *268*, 190–197. [[CrossRef](#)]
14. Maruszczuk, A.; Dudek, A.; Szala, M. Research into Morphology and Properties of  $\text{TiO}_2$ -NiAl Atmospheric Plasma Sprayed Coating. *Adv. Sci. Technol. Res. J.* **2017**, *11*, 204–210. [[CrossRef](#)]
15. Hejwowski, T.; Łabacz-Kęćik, A. Mikrostruktura i odporność na zużycie powłok natryskiwanych metodą płomieniowo-proszkową mieszaninami proszków. *Przegląd Spaw.-Weld. Technol. Rev.* **2012**, *9*, 57–64. [[CrossRef](#)]

16. Hejwowski, T. Comparative study of thermal barrier coatings for internal combustion engine. *Vacuum* **2010**, *85*, 610–616. [[CrossRef](#)]
17. Chen, J.; Zhou, H.; Zhao, X.; Chen, J.; An, Y.; Yan, F. Microstructural Characterization and Tribological Behavior of HVOF Sprayed NiMoAl Coating from 20 to 800 °C. *J. Therm. Spray Technol.* **2015**, *24*, 348–356. [[CrossRef](#)]
18. Hou, G.; Zhao, X.; Zhou, H.; Lu, J.; An, Y.; Chen, J.; Yang, J. Cavitation erosion of several oxy-fuel sprayed coatings tested in deionized water and artificial seawater. *Wear* **2014**, *311*, 81–92. [[CrossRef](#)]
19. Santa, J.F.; Espitia, L.A.; Blanco, J.A.; Romo, S.A.; Toro, A. Slurry and cavitation erosion resistance of thermal spray coatings. *Wear* **2009**, *267*, 160–167. [[CrossRef](#)]
20. Ksiazek, M.; Boron, L.; Radecka, M.; Richert, M.; Tchorz, A. Mechanical and Tribological Properties of HVOF-Sprayed (Cr<sub>3</sub>C<sub>2</sub>-NiCr+Ni) Composite Coating on Ductile Cast Iron. *J. Mater. Eng. Perform.* **2016**, *25*, 3185–3193. [[CrossRef](#)]
21. Kekes, D.; Psyllaki, P.; Vardavoulias, M.; Vekinis, G. Wear micro-mechanisms of composite WC-Co/Cr-NiCrFeBSiC coatings. Part II: Cavitation erosion. *Tribol. Ind.* **2014**, *36*, 375–383.
22. Hejwowski, T. Wear resistance of graded coatings. *Vacuum* **2002**, *65*, 515–520. [[CrossRef](#)]
23. ISO 4287:1997. *Geometrical Product Specifications (GPS)—Surface texture: Profile method—Terms, definitions and surface texture parameters*; International Organization for Standardization: Geneva, Switzerland, 1997.
24. Steller, J. International Cavitation Erosion Test and quantitative assessment of material resistance to cavitation. *Wear* **1999**, *233–235*, 51–64. [[CrossRef](#)]
25. Hattori, S.; Ishikura, R.; Zhang, Q. Construction of database on cavitation erosion and analyses of carbon steel data. *Wear* **2004**, *257*, 1022–1029. [[CrossRef](#)]
26. *ASTM G32-10: Standard Test Method for Cavitation Erosion Using Vibratory Apparatus*; ASTM International: West Conshohocken, PA, USA, 2010.
27. Tucker, R.C. *ASM Handbook Volume 5A: Thermal Spray Technology*; ASM International: Geauga County, OH, USA, 2013; ISBN 978-1-61503-996-8.
28. Shaw, L.L.; Goberman, D.; Ren, R.; Gell, M.; Jiang, S.; Wang, Y.; Xiao, T.D.; Strutt, P.R. The dependency of microstructure and properties of nanostructured coatings on plasma spray conditions. *Surf. Coat. Technol.* **2000**, *130*, 1–8. [[CrossRef](#)]
29. Szala, M. Application of computer image analysis software for determining incubation period of cavitation erosion – preliminary results. In *ITM Web of Conferences, Proceedings of the II International Conference of Computational Methods in Engineering Science (CMES'17), Lublin, Poland, 23–25 November 2017*; EDP Sciences: Reyulis, France, 2017; Volume 15, p. 06003. [[CrossRef](#)]
30. Dybowski, B.; Szala, M.; Hejwowski, T.J.; Kielbus, A. Microstructural phenomena occurring during early stages of cavitation erosion of Al-Si aluminium casting alloys. *Solid State Phenom.* **2015**, *227*, 255–258. [[CrossRef](#)]
31. Tomlinson, W.J.; Kalitsounakis, N.; Vekinis, G. Cavitation erosion of aluminas. *Ceram. Int.* **1999**, *25*, 331–338. [[CrossRef](#)]

